Review of Scientific Instruments

Laser heating setup for diamond anvil cells for *in situ* synchrotron and in house high and ultra-high pressure studies

Cite as: Rev. Sci. Instrum. **90**, 104501 (2019); https://doi.org/10.1063/1.5117786
Submitted: 01 July 2019 . Accepted: 12 September 2019 . Published Online: 04 October 2019

T. Fedotenko, L. Dubrovinsky, G. Aprilis, E. Koemets, A. Snigirev, I. Snigireva, A. Barannikov, P. Ershov, F. Cova, M. Hanfland, and N. Dubrovinskaia

AIP Publishing

Review of Scientific Instruments ARTICLE scitation.org/journal/rsi

Laser heating setup for diamond anvil cells for *in situ* synchrotron and in house high and ultra-high pressure studies

Cite as: Rev. Sci. Instrum. 90, 104501 (2019); doi: 10.1063/1.5117786
Submitted: 1 July 2019 • Accepted: 12 September 2019 •
Published Online: 4 October 2019

T. Fedotenko,[1,a)] L. Dubrovinsky,[2] G. Aprilis,[1] E. Koemets,[2] A. Snigirev,[3] I. Snigireva,[4] A. Barannikov,[3] P. Ershov,[3] F. Cova,[4] M. Hanfland,[4] and N. Dubrovinskaia[1]

AFFILIATIONS

[1]Material Physics and Technology at Extreme Conditions, Laboratory of Crystallography, University of Bayreuth, D-95440 Bayreuth, Germany
[2]Bayerisches Geoinstitut Universität Bayreuth, D-95440 Bayreuth, Germany
[3]Immanuel Kant Baltic Federal University, 236041 Kaliningrad, Russian Federation
[4]European Synchrotron Radiation Facility, F-38043 Grenoble, France

[a)]**Author to whom correspondence should be addressed:** TimofeyFedotenko@gmail.com

ABSTRACT

The diamond anvil cell (DAC) technique combined with laser heating is one of the major methods for studying materials at high pressure and high temperature conditions. In this work, we present a transferable double-sided laser heating setup for DACs with *in situ* temperature determination. The setup allows precise heating of samples inside a DAC at pressures above 200 GPa and could be combined with synchrotron beamline equipment. It can be applied to X-ray diffraction and X-ray transmission microscopy experiments. In the setup, we use high-magnification and low working distance infinity corrected laser focusing objectives that enable us to decrease the size of the laser beam to less than 5 μm and achieve the maximum optical magnification of 320 times. All optical components of the setup were chosen to minimize chromatic and spatial aberrations for accurate *in situ* temperature determination by multiwavelength spectroscopy in the 570–830 nm spectral range. Flexible design of our setup allows simple interchange of laser sources and focusing optics for application in different types of studies. The setup was successfully tested in house and at the high-pressure diffraction beamline ID15B at the European Synchrotron Radiation Facility. We demonstrate an example of application of the setup for the high pressure–high temperature powder diffraction study of PdH and X-ray transmission microscopy of platinum at 22(1) GPa as a novel method of melting detection in DACs.

I. INTRODUCTION

Laser heating (LH) in diamond anvil cells (DACs) has been used for more than five decades,[1,2] and there are many examples of its applications in geosciences for simulating the conditions of deep Earth's and planetary interiors, studies of physical and chemical processes at extreme conditions, and synthesis of novel materials.[3–7] The methodology of laser-heated diamond anvil cells (LHDACs) is well described in the literature.[8] Over the last decade, this technique has evolved into a useful and routine experimental method at synchrotron beamlines. The LHDAC technique has been coupled with different analytical methods such as powder and single crystal X-ray diffraction[9] (XRD), X-ray absorption spectroscopy (XAS),[10,11] nuclear inelastic scattering,[12] and synchrotron Mössbauer source (SMS).[13]

Dynamic development of the LHDAC technique during recent years has resulted in the emergence of portable laser heating systems which can be used for *in house* experiments in different scientific environments (i.e., simultaneously with resistivity measurements, Raman, or Brillouin spectroscopy), are easily moved between synchrotron beamlines, and coupled with different analytical techniques in response to modern scientific challenges. The first portable laser heating system was invented by Boehler in 2009[8] and was successfully tested in XRD and XAS experiments at the

synchrotron source. The one-side LH setup developed by Dubrovinsky *et al.*[14] was successfully used for in house[15] studies and synchrotron *in situ* X-ray absorption and single crystal XRD experiments.[16] However, the single-side heating leads to large temperature gradients within the samples that limit applications of the setup for thin samples.

The designs of the double-sided LH systems described by Kupenko *et al.*[13] and Aprilis *et al.*[17] are based on universal laser-heating heads (UniHeads, adapted finite cutting laser heads produced commercially by Precitec GmbH & Co. KG), which enable us to decrease the size of a laser heating setup. The setups[13,17] are simple to install and may be used in experiments which require the rotation of DACs during data collection (particularly, for single-crystal XRD in laser-heated DACs).

The UniHead-based LH setups allow varying the size of the laser beam from 15 to 50 μm FWHM and providing 20 times magnification of the samples in DACs, which is sufficient for the majority of conventional experiments with laser heating. However, in ultra-high pressure diamond anvil cells (with beveled anvils with small culet sizes, double-stage-, or toroidal-type anvils, for example), the size of the pressure chamber is usually smaller than 15 μm and above 200 GPa samples, as a rule, are of about 3–4 μm in diameter. This requires tighter laser beam focusing, higher magnification, and better optical resolution. Moreover, even when using specially designed objectives (such as GeoHeat 40_NIR), it is hard to reduce chromatic and spatial aberrations introduced by commercial optical elements of UniHeads (especially in the case of tight focusing) that could be crucial for temperature determination in laser heating experiments at temperatures above 3000 K.

In this paper, we present a transportable double-sided laser-heating setup for *in house* and synchrotron experiments. It is designed to improve the accuracy of temperature measurements, to decrease the size of the laser spot focused on the sample, and to get higher magnification for precise heating in DACs at pressures above 200 GPa.

We demonstrate its application on examples of an *in situ* powder X-ray diffraction experiment and *in situ* X-Ray Transmission Microscopy (XRTM) imaging at the ID15B beamline of the European Synchrotron Radiation Facility (ESRF) and a series of in house experiments with the heating of samples in DACs above 200 GPa.

II. DESIGN OVERVIEW

A. General overview

The system consists of two identical parts which are schematically shown in Fig. 1.

Each of the parts includes the following nodes:

- Near-infrared (NIR) laser
- Power control module based on two polarized beam splitters and half-wave plate
- Focusing and shaping optics
- Observation module
- Temperature collection module

All major nodes are mounted on the breadboard, and all optical components can be easily adjusted or modified depending on a type or specific needs of experiments.

B. Lasers

Independence of the different nodes of the system allows us to quickly exchange the laser sources for experiments at a synchrotron facility or for heating at the home institute (i.e., laser sources do not need to be transferred together with the laser-heating setup); however, the central wavelength of laser emission should be in the range of 1050–1070 nm because all of the shaping and focusing optics described below are configured to work in this range.

The setup was tested with two different pairs of lasers. Each of the two SPI RedPower R4 modulated fiber lasers of the first pair, one

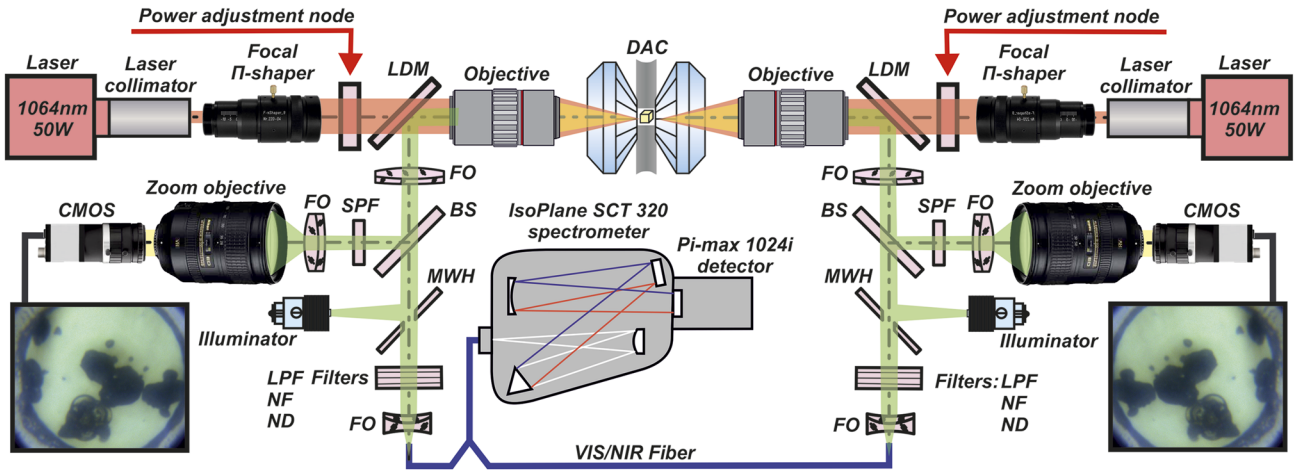

FIG. 1. Schematic diagram of the double-sided laser heating system for diamond anvil cells. LDMs are the long-pass dichromic mirrors; FOs are the focusing optics; BSs are 50/50 beam splitters; SPFs are the short-pass filters with a cutoff at 800 nm; CMOSs are the cameras for optical observation; MWHs are the mirrors with a hole; LPFs are the long-pass filters with a cut-on wavelength of 550 nm; NFs are the notch filters at 1064 nm; and NDs are neutral density filters.

with a maximum power of 100 W and the other with 50 W, emits a randomly polarized Gaussian beam (TEM_{00}) with a full width at the $1/e^2$ of 5 ± 0.5 mm (the central wavelength is 1070 ± 10 nm). The lasers can be operated in two modes: in a continuous-wave (CW) mode or in a modulated with maximum frequency up to 100 KHz. The second pair of lasers is SPI G4 pulsed fiber lasers with a maximum output power up to 50 W and central emission wavelength at 1064 nm ± 10 nm. Each one has randomly polarized Gaussian beam (TEM_{00}) with an output beam diameter of 10 mm and divergence 120 μrad. The lasers can be operated in both continuous-wave and pulsed modes. The minimum possible laser pulse of the FWHM is 11 ns.

For both laser pairs, the output power level can be controlled by an external graphical user interface (GUI), provided by the manufacturer. However, working in a low-power CW mode (power below 5 W) or working in short-pulse mode significantly increases the power control error of the laser feedback loop and strongly demands an external power control. For the accurate power control, we use an external analog optical controller, which will be described in detail in Sec. II D.

Lasers are equipped with an additional low-power red laser source (630–680 nm) for preliminary beam alignment and positioning on the sample.

C. Beam shaping and focusing

The setup demands focusing optics that can simultaneously operate in two spectral bands: NIR for focusing of the laser beam, and the optical range for collection of thermal emission and imaging of the sample.

Both sides of the LH setup are equipped with specially designed TEM_{00} focal-π shapers (Focal-π Shaper_9_1064 by AdlOptica GmbH) to expand the output collimated laser beam and convert its initially spatial Gaussian distributed intensity to a flat-top π-shape profile.

To focus the laser beam in synchrotron experiments, we use a GeoHeat 40_NIR achromatic objective specially designed for laser heating applications in DACs. The GeoHeat 40_NIR working distance is 80 mm that provides enough space around a DAC for inserting additional optics to target the laser beam on a sample that is essential for *in situ* synchrotron X-ray diffraction and imaging in LHDAC studies. It minimizes chromatic aberrations in the spectral range of 600–900 nm used for temperature measurements and focuses the NIR laser beam.[17,18]

By adjusting the focal-π shaper, we reach the smallest FWHM of the laser beam of 20 μm, for a flat-top profile used, and 10 μm FWHM for a Gaussian shaped laser beam.

Experiments with ultrahigh pressure DACs require tighter laser beam focusing, higher magnification, and better optical resolution as far as the size of a sample could be less than 5 μm. To overcome these challenges, we use a Mitutoyo 20x objective (Mitutoyo NIR infinity corrected M Plan Apo B 20x) on both sides of the setup. Likewise, GeoHeat 40_NIR, the Mitutoyo 20x objective, works in optical and NIR spectral ranges and allows focusing the laser beam to 5 μm FWHM on a sample. However, the working distance of the Mitutoyo 20x is 25 mm that does not provide enough space between the end of the objective and a DAC and makes it inapplicable for *in situ* synchrotron experiments.

D. Power control node

It is well known that in pulsed fiber lasers, there is a strict relation between the pulse shape and the energy. Therefore, pulsed LHDAC experiments require an independent control of the laser pulse shapes and the energy of the individual pulses in order to provide stable heating and to avoid damaging the diamond anvils. The hardware control of the laser power in the CW mode does not allow access to the low-power region (between 0 and 5 W).

To resolve this problem, in our setup, we used the polarization-based power control module schematically presented in Fig. 2. The module consists of two polarized NIR beam splitters (Thorlabs CCM1-PBS25-1064) and a half-wave plate (Thorlabs WPH05M-1064) mounted between them. The output power level is controlled by the rotation of the λ/2 wave plate in the range from 0° to 45° to reach zero and maximum power, correspondingly. The part of laser radiation rejected from the beam splitters is dissipated on graphite-based beam blocks (Thorlabs LB2/M) to satisfy the safety regulations.

E. Observation

For imaging of the sample, we use high-resolution EYE © CMOS cameras (UI-3240CP), while the sample is illuminated by the LED (Thorlabs MCWHLP1). The image of the sample is obtained either in transmitted light, if a material in the sample chamber is at least partially transparent, or/and in reflected light. The light passes through a set of lenses into a zoom objective (Nikon AF-S NIKKOR 28–300 mm f/3.5–5.6G ED VR Lens) projecting the

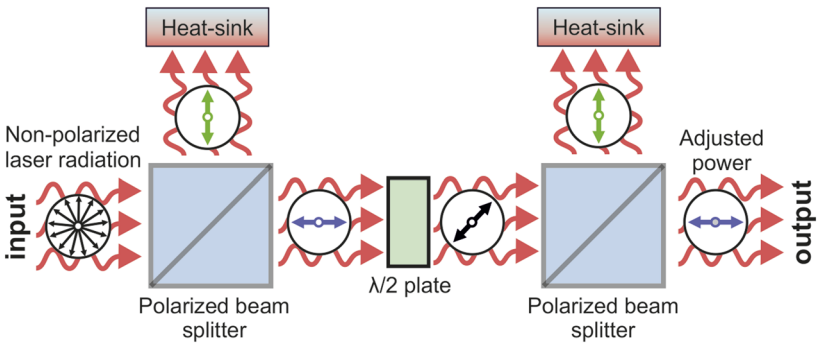

FIG. 2. Working principle of the power control node.

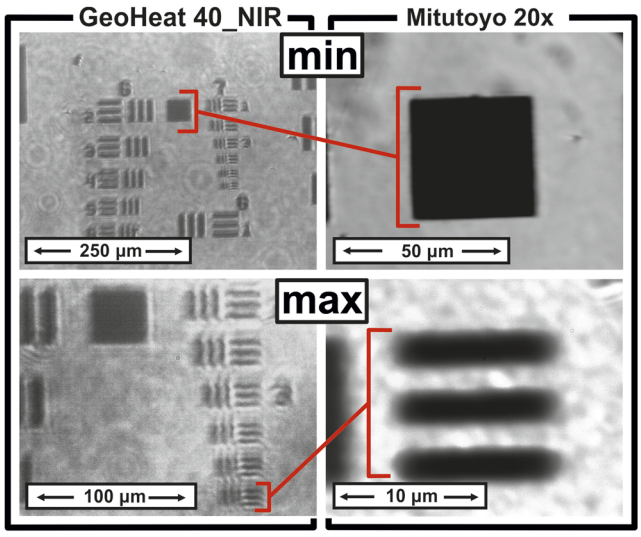

FIG. 3. The images of the test target plate at minimum and maximum magnification for GeoHeat 40_NIR and Mitutoyo 20x objectives.

image of the sample on the matrix of a CMOS camera. A short pass filter (Edmund #47–586) with a cutoff at 800 nm is placed in front of the zoom objective to protect the CMOS camera from laser reflections.

To determine the magnification of the optical system, we imaged the positive test target (Thorlabs R1DS1P, conformed to MIL-S-150A standard) with a maximum resolution of 228 lines per millimeter. The images of the test target for both objectives (GeoHeat_40 NIR and Mitutoyo NIR infinity corrected M plan Apo B 20x) are presented in Fig. 3. GeoHeat_40_NIR enables the magnification to be varied within approximately 20–35 times, while Mitutoyo 20x provides 80–320 times magnification. The spatial resolution of the final image with the GeoHeat 40_NIR objective is limited to approximately 180 lines per millimeter at maximum magnification; Mitutoyo 20x provides spatial resolution higher than 228 lines per millimeter, which is the limit for the used test target.

F. Thermal radiation collection

Minimization of the optical distortions introduced by optical elements (lenses, beam splitters, and filters) encountered by emitted radiation on the way to the spectrometer is necessary for precise temperature measurements in LHDAC experiments, and it is one of the primary goals for the designed setup.

To separate laser and optical observation/collection paths, we use a Thorlabs DMLP900 dichroic mirror that reflects the visible wavelength light and transmits the laser-frequency light. The DMLP900 provides a flat top reflection spectral profile in the range of 600–850 nm. A 50/50 beam splitter (Thorlabs BSW10) installed on the observation path reflects half of the light intensity to the spectrometer for the temperature measurements, and the other half of the light intensity goes eventually to the CMOS camera for simultaneous visual observations. The thermal radiation reflected by the beam splitter is focused on the optical fiber by an additional lens (Edmund #45–220) and guided into an IsoPlane SCT 320 spectrometer with a 1024x256 PI-MAX 4 camera (Princeton Instruments, Inc.). To prevent saturation of the detector by diffused laser radiation, we use a blocking notch filter with a central wavelength of 1064 nm (Edmund #86–128). For precise temperature measurements above 4500 K, a long-pass filter with the edge at 550 nm (Thorlabs FEL0550) is installed to avoid contamination of thermal emission spectra by second-order UV reflections.

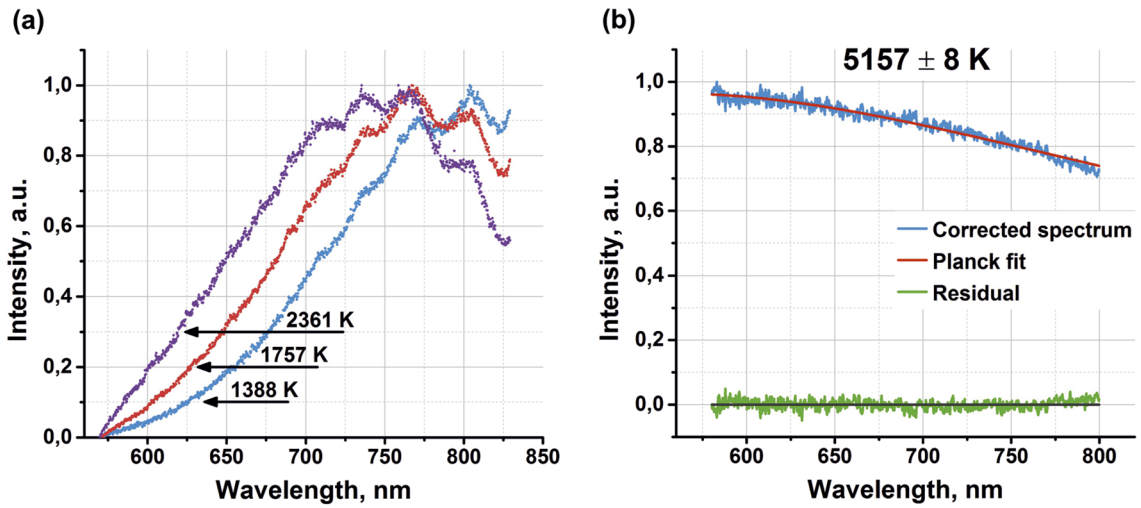

FIG. 4. Temperature determination procedure. (a) Normalized spectra of a calibration lamp at 1388, 1757, and 2361 K. (b) Example of temperature determination of heated silicate perovskite ($Fe_{0.5}Mg_{0.5}Si_{0.5}Al_{0.5}O_3$) at 65(2) GPa inside a DAC using the gray body approximation of Planck's law. Error of measured temperature corresponds to the standard deviation from the fit.

Calibration of the system's response is performed by using calibrated tungsten lamps at temperatures of 1388, 1757, and 2361 K. The noncorrected spectra of a calibration lamp are presented in Fig. 4(a). Once the emission spectra are corrected and the effects introduced by optical components removed, the temperature can be determined by fitting the spectra in a given wavelength range (600–800 nm) to the Plank radiation function. Figure 4(b) demonstrates an example of fitting of thermal radiation spectra collected during heating of silicate perovskite ($Fe_{0.5}Mg_{0.5}Si_{0.5}Al_{0.5}O_3$) at 65(2) GPa inside a DAC.

III. EXAMPLES OF APPLICATION

A. Ultrahigh pressure LH

In conventional LH-DAC experiments, the size of the laser beam is ranged from the 10 to 50 μm FWHM. However, LH-DAC experiments at pressures over 200 GPa require tighter focusing of the laser beam as far as the size of the sample is of about 3–4 μm in diameter. Furthermore, to distinguish the sample from the environment during the heating, it is necessary to have high magnification and optical resolution of the image projected on the camera sensor.

During in house LH experiments, the setup is mounted on the optical table as shown in Fig. 5.

The setup was successfully tested in DAC experiments with 40-μm culet size anvils (pressure chambers are about 10–20 μm in diameter, characteristic sample sizes of about 5 μm) at pressures over 200 GPa. Figure 6 shows an image of the DAC pressure chamber during laser heating of NiO in a Ne pressure medium at 230(5) GPa and 2500 ± 150 K.

B. Combination with synchrotron techniques

The transportability of the system was demonstrated during a series of experiments using X-ray diffraction and imaging at the synchrotron X-ray source coupled with the LHDAC at the high pressure diffraction beamline (ID15B) of the European Synchrotron Radiation Facility (ESRF). The system was transported to the ESRF and mounted in the experimental hutch of the beamline. The system's assembling and alignment take 8–10 hours prior to the experiment. To save experimental time, the installation can be performed in advance, during a maintenance time or shut down.

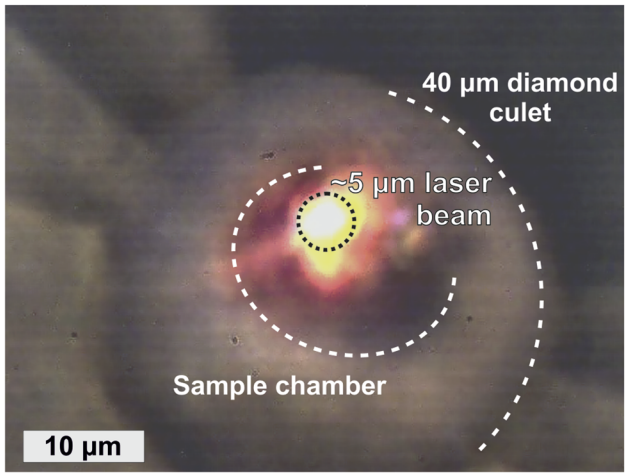

FIG. 6. Image of the sample chamber during laser heating of NiO in Ne as pressure transmitting medium at 230(5) GPa and 2700 ± 150 K. Beveled diamond anvils have a culet size of 40 μm in diameter.

The geometry of the system was partially modified for synchrotron use (Fig. 7) to enable simultaneous XRD and LH. All major nodes of the LH setup from the upstream [labeled (5) in Fig. 7] and downstream [labeled (6) in Fig. 7] sides were mounted on optical breadboards and installed on movable 3-axis stages. In lack of free space close to the 3D-stage with the DAC, focusing and targeting optics [labeled (4) in Fig. 7] were installed on rails and placed 300 mm away from main breadboards.

To direct the laser beam to the sample from both sides of the DAC, we used two graphite mirrors placed in front of each of the GeoHeat 40_NIR objectives (Fig. 8). As X-ray absorption of the carbon mirror is low, there is no problem if X-rays hit the mirror at the upstream side, which is positioned at ~45° to both the laser beam and the X-ray beam. From the downstream side, the mirror is placed at ~40° to the laser beam to prevent X-rays from heating the mirror

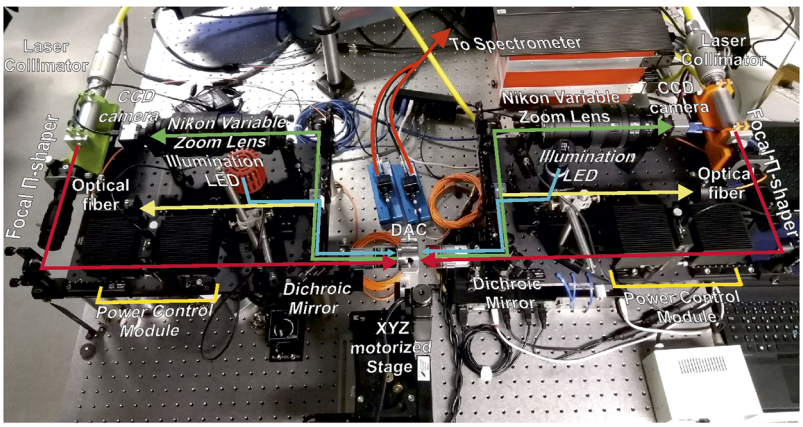

FIG. 5. Configuration of the LH setup for in house experiments.

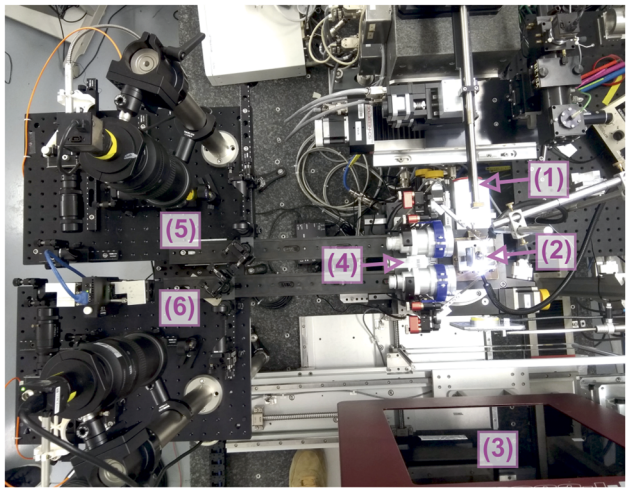

FIG. 7. (1) X-ray beam pinhole, (2) DAC, (3) Mar555 detector, (4) focusing and targeting optics, (5) upstream breadboard, and (6) downstream breadboard.

and to avoid diffuse scattering from carbon. For precise positioning of the laser beam on the sample during the experiment, both mirrors were fixed on piezomirror mounts (Newport 8821).

1. Synthesis and behavior of palladium hydride (PdH) at high P-T

Palladium is a transition metal well known for its exceptional ability to absorb hydrogen in the bulk,[19,20] forming fcc–structured PdH_x compounds. Along with some other transition metal polyhydrides, palladium hydrides PdH_x are known for their superconducting properties.[21–23]

As a part of our studies of the Pd-H system at high pressure, we investigated the behavior of PdH_x at high P-T conditions using the LHDAC with *in situ* synchrotron X-ray diffraction. To synthesize this palladium hydride, a piece of Pd foil was loaded inside a sample chamber of a BX90-type diamond anvil cell equipped with Boehler–Almax type diamonds (culet diameter 250 μm) and a rhenium gasket. To form the sample chamber, a rhenium gasket was preindented to 25 μm thickness and a hole of 100 μm in diameter was drilled in the center of the indentation. Paraffin oil was used as both a pressure-transmitting medium and a source of hydrogen for the synthesis. The sample was compressed up to 39(2) GPa and laser-heated from both sides at 1500 ± 100 K. The fcc-structured PdH_x formed due to a reaction between Pd and paraffin oil. The unit cell parameter was found to be 60.18 ± 0.05 Å^3 from synchrotron X-ray diffraction data (Fig. 9) obtained at the ID15B synchrotron beamline at the ESRF (λ = 0.4117 Å, Mar555 flat panel detector). The X-ray diffraction images at ambient temperature were collected during continuous rotation of the DAC from −20° to +20° ω.

Within the uncertainty of experimental data, the unit cell volume of synthesized PdH_x (60.18 ± 0.05 Å^3) is consistent with that for PdH (x = 1) (60.1 ± 0.1 Å^3) calculated from the PdH equation of state;[24] thus, we consider for our sample x to be equal to 1. As shown in Fig. 9, after heating, not only palladium hydride but also diamond could be detected in the pressure chamber.

To check the stability of the synthesized PdH under high P-T conditions, we collect X-ray diffraction during LH at 2000 ± 200 K and 39(2) GPa. The diffraction pattern of the sample at 2000 ± 200 K [Fig. 10(a)] does not have any other reflections aside from those of cubic PdH and diamond. The unit cell parameters of palladium hydride before and after heating appeared to be the same [Fig. 10(b)] that could give evidence that the amount of hydrogen in PdH did not change during heating and the shift of the position of the (111) reflection of cubic PdH upon heating to

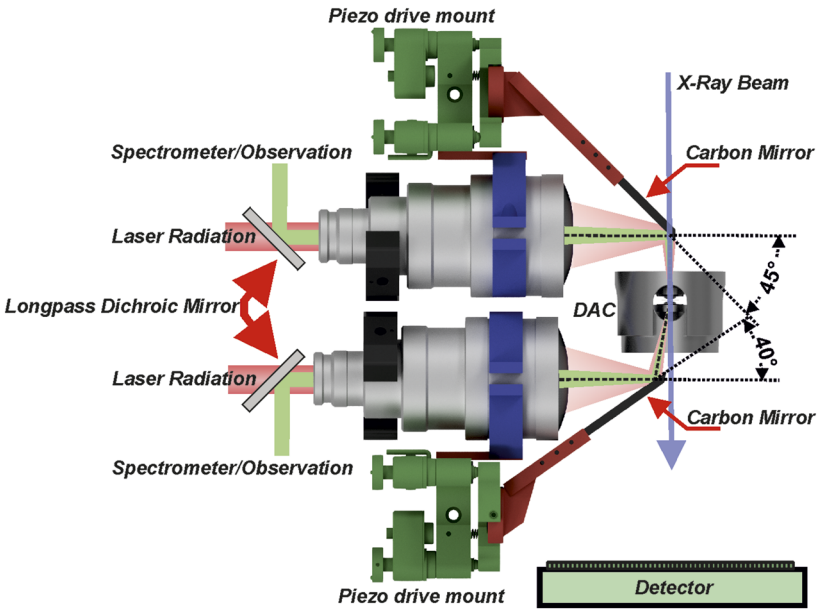

FIG. 8. Scheme of the laser beam targeting on the sample inside the DAC in experiments with synchrotron X-ray radiation at ID15B (ESRF). The upstream carbon mirror is positioned at ~45° to the laser beam. To prevent X-rays from hitting the mirror resulting in diffuse scattering from carbon on the detector, the downstream mirror is positioned at ~ 40° to the laser.

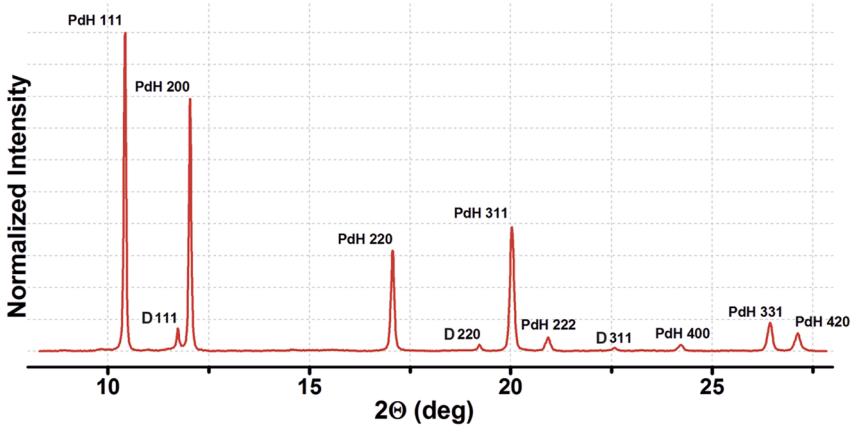

FIG. 9. A diffraction pattern of palladium hydride at 39 (2) GPa and ambient temperature. The fcc PdHx (x ≈ 1) along with diamond was formed after laser heating of Pd in paraffin at 1500 ± 200 K and 39(2) GPa. Indexes of the diffraction peaks of palladium hydride (PdH) and diamond (D) are designated (λ = 0.4117 Å). The unit cell volume of PdH is 60.18 ± 0.05 Å^3.

2000 ± 200 K at 39(2) GPa was attributed only to expansion of the PdH lattice.

According to the XRD, the unit cell volume increased from 60.18(5) A^3 at room temperature (298 K) to 60.42(5) A^3 at 2000 ± 200 K. This gives for PdH at 39(2) GPa a volumetric thermal expansion coefficient of 2.3 (±0.4) 10^{-6} 1/K, which is significantly lower than that of Pt (20.1(±0.5) 10^{-6} 1/K)[25] at similar conditions (39 GPa at heating up to 1900 K). To our knowledge, the thermal behavior of Pd and Pd-hydrides at high pressure has not been studied so far; therefore, we compare our data with those known for Pt, as the thermal expansion of Pt is close to that of Pd at atmospheric pressure. One of the possible explanations of the observed large difference in the thermal expansion coefficients of Pt and PdH at high pressure can be related to the chemical behavior of PdH on heating. Indeed, if PdH loses hydrogen at high temperature, this should lead to a decrease in the unit cell volume, compensating for the effect of the thermal expansion, and thus effectively lowers the thermal expansion coefficient. During cooling, hydrogen can be accommodated up to the same amount as before. Thus, there is a possibility that the effect of the volume change under heating cannot be exclusively attributed to the thermal expansion.

2. In situ X-ray transmission microscopy in LH-DACs

In this part, we describe the application of our transportable laser-heating setup for visualization of processes in the DAC at high temperature using X-Ray Transmission Microscopy (XRTM). Particularly, on the beamline ID15B (ESRF), we observed *in situ* melting of platinum in a DAC at high pressures.

Several methods of detection of melting in laser-heated DACs are known. In particular, it can be done due to optical observations, XRD, X-ray absorption, or Raman measurements.[8,26–28] Search for signs of melting on surfaces of recovered materials using scanning electron microscope and focus ion beam techniques, put forward by Boehler *et al.*,[29,30] is helpful, but time and labor consuming. Moreover, distinguishing between melting and recrystallization textures, and the analysis of possible chemical

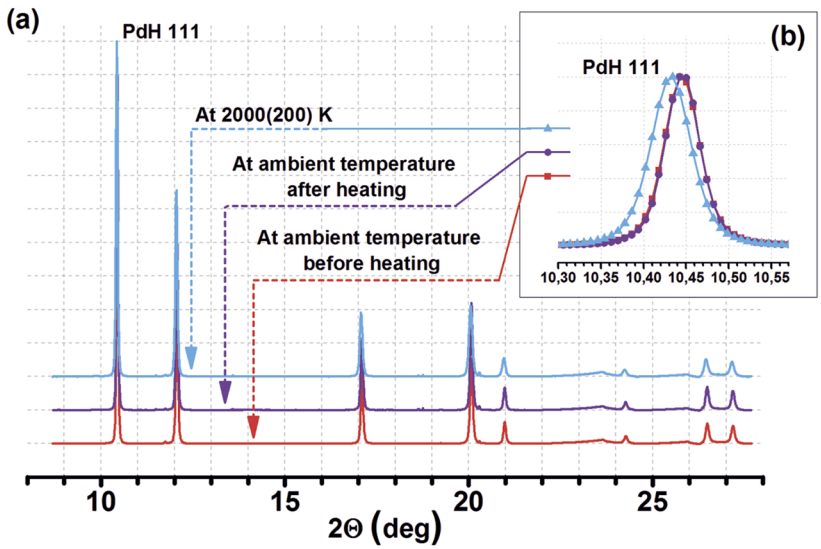

FIG. 10. (a) The diffraction patterns of the PdH sample at 39(2) GPa. (b) Shift of the position of the (111) reflection of the cubic PdH upon heating to 2000 ± 200 K at 39(2) GPa. The position of the (111) reflection remains the same before and after heating (λ = 0.4117 Å).

contamination by carbon are not always trivial. Considerable difficulties associated with detection of melting at high pressures result in significant inconsistencies in reported melting curves for the same materials.[31,32]

Each of the current methods of melting detection in LHDACs is associated with specific challenges, which can lead to ambiguities. *In situ* melting detection at temperatures above ~2000 K is possible by visual observation of fluid motion in a speckle interference pattern[33] but linked to the subjective judgment of the observer.[34] The image analysis procedure for the quantification of changes in the speckle interference pattern appeared last years.[35] Identification of melting using X-ray diffraction is in general possible at synchrotron beamlines with an appropriate setup.[27,28] In this case, melting is manifested either by disappearance of Bragg reflections and/or by appearance of diffuse scattering due to the short-range order in the liquid state. However, the disappearance of reflections on still X-ray images may be a result of recrystallization (without melting) of the sample.[31] In order to produce a detectable signal, the amount of melted liquid in the sample should be significant and the melt has to be stable for some time in a complex and highly thermally and chemically inhomogeneous environment of the DAC. Moreover, experiments can be complicated due to possible chemical reactions with the pressure medium or the diamond anvils.[36,37] The detection of melting using X-ray absorption suffers from at least the same problems.

The development of XRTM using compound refractive lenses (CRL) at ID15B opened up new perspectives for studies in DACs. We demonstrated,[38,39] particularly, that with XRTM, it is possible to get an image with submicron resolution, which is hardly possible with conventional optics in the visual light.

An X-ray energy of 30 keV was selected using a cryogenically cooled Si (111) horizontally deflected monochromator with $\Delta\lambda/\lambda \sim 10^{-4}$. Transmission X-ray microscopy was realized using compound refractive lenses (CRL),[40] according to the scheme shown in Fig. 11. The design of the beamline allows us to translate the diffraction detector out of the beam and to introduce an additional X-ray objective lens to perform X-ray microscopy. The objective lens assembly was consisted of 66 aluminum and 45 beryllium parabolic refractive lenses. The lenses of both types have the radius of parabola apex of 50 μm. The objective lens was placed on the stage with all necessary translations and rotations needed for the lens alignment. The DAC was located at a distance of 50 cm in front of the objective. X-ray images were recorded with a high resolution PCO X-ray CCD camera with 0.74 μm pixel size, which was installed at the distance of about 5 m from the DAC. Therefore, the magnification of about 10 was achieved. The transfocator that was located at 44 m from the undulator, was used to provide appropriate illumination on the sample.[41–43] It should be noted that it is very important to match the illumination area on the sample with sample sizes during microscopy experiments. This was achieved by varying the number of lenses in the transfocator. Such an experimental arrangement allows us to preserve beam coherence and gives unique opportunities for the realization of X-ray phase contrast microscopy with a spatial resolution down to 200 nm.[38,39,44–46]

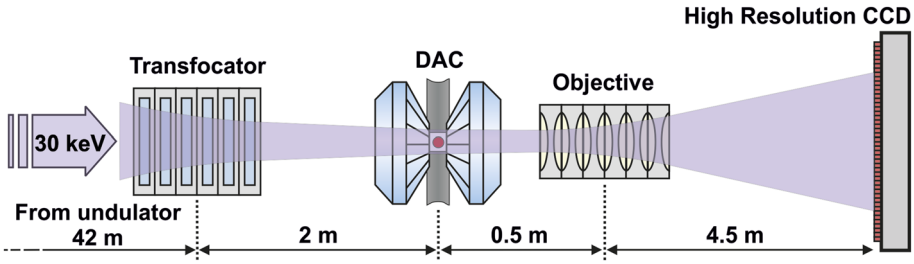

FIG. 11. Experimental layout for X-ray microscopy experiments.

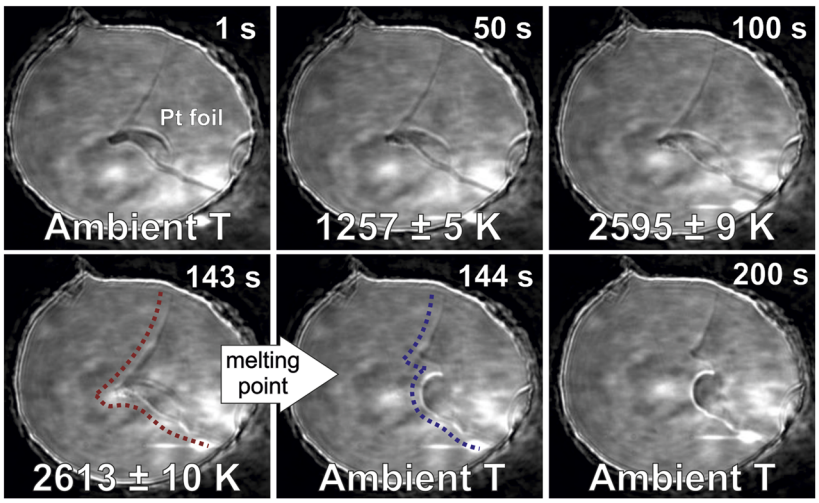

FIG. 12. XRTM images of the sample chamber taken during the heating process. Each image was collected with 1 s exposure time. Red and blue dotted lines represent the shape of the Pt foil before and after melting, respectively. The melting moment was detected between the 143rd and 144th s by the observation of the Pt foil shape. The melting temperature of Pt at 22 (1) GPa is 2613 ± 10 K. Presented errors correspond to the standard deviation from the fit.

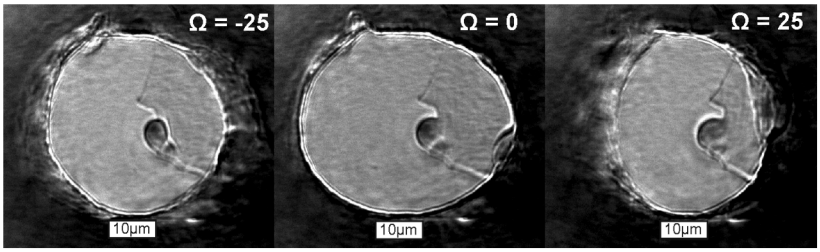

FIG. 13. XRTM images of the DAC sample chamber at different angular orientations of the DAC. Multimedia view: https://doi.org/10.1063/1.5117786.1.

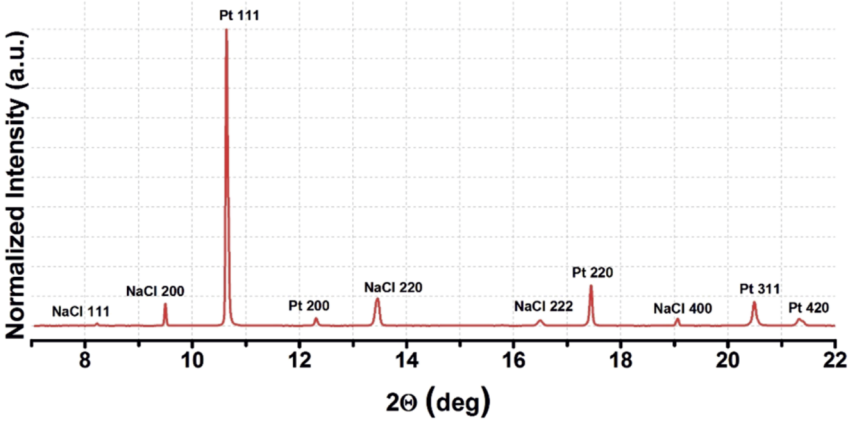

FIG. 14. The diffraction pattern taken from the melted area of the sample at 22(1) GPa after heating. Pure Pt and B1-NaCl are the only materials detected by XRD.

X-ray phase contrast microscopy allows us to monitor the position and size of the sample; map the sample and find the area of interest; investigate the morphology of the sample during phase transitions, chemical reactions, or melting of the sample; and study mechanical stresses in DACs and a failure mechanism under ultrahigh pressures. It is necessary to point out that the proposed beamline concept can be easily adapted for the upgraded Extremely Brilliant Source (EBS) simply by changing the number of individual lenses in the transfocators.

To demonstrate the feasibility of *in situ* XRTM in LHDACs, we performed an experiment aiming to detect the melting of Pt. Platinum was chosen because it is chemically inert, and possible chemical reactions that could affect the result can be excluded. The relatively low melting temperature of Pt simplifies the experiment, and its melting curve has been already experimentally established.[47] A piece of Pt foil was clamped between two thin layers of NaCl from both sides and loaded inside a sample chamber of a BX90-type diamond anvil cell equipped with Boehler–Almax type diamonds (with a culet diameter of 250 μm). To form the sample chamber, a rhenium gasket was preindented to 25 μm thickness and a hole with a 110-μm diameter was drilled in the center of the indent. NaCl was used as a pressure-transmitting medium and a thermal insulator to minimize the dissipation of heat through the diamonds. The sample was compressed up to 22(1) GPa.

We heated the sample for 200 s simultaneously recording a series of XRTM images with 1-s exposure time and measuring the temperature using spectroradiometry. Figure 12 presents the XRTM images of the sample during the heating, and as seen the sample changes its shape and texture.

For the first 143 s, the laser power was slowly increasing. A significant change of the shape of Pt foil caused by its melting was detected between 143th and 144th s. We observe the formation of the Pt droplet (the size is around 10 μm) from initial Pt foil, which excludes simple recrystallization. XRTM tomography collected after LH proves the formation of a droplet, which is shown in Fig. 13 (Multimedia view).

Before melting event, all visual changes in the texture and shape of the Pt foil were caused by warming up the sample chamber and its relaxation. The temperature collected at the last moment before melting was 2613 (10) K. After melting, the sample moved out of the laser beam and no thermal emission was present.

The diffraction pattern of the heated area recorded after LH is presented in Fig. 14. It proves the absence of a chemical interaction between the Pt sample and its surrounding. The melting temperature of Pt at 22(1) GPa (2613 ± 10 K) obtained in the experiment described above due to a combination of XRTM and LH-DACs is in good agreement with the literature data (2583 ± 97 K).[47]

IV. CONCLUSION

A transportable double-sided laser heating system enabling simultaneous visual observation of a sample and its heating and temperature measurements has been developed. The configuration of the system can be easily changed: the geometry and optical components can be modified for any specific needs. Use of Mitutoyo 20× objectives as focusing optics for in-house experiments allows us to decrease the beam size of the laser beam to 5 μm and improves the

optical quality of imaging that opens new opportunities in LHDAC experiments at pressures above 200 GPa. Using conventional Nikon camera lenses as zoom objectives allows varying the optical magnification of the setup from 80 to 320 times with optical resolution significantly higher than 228 lines per millimeter. For accurate temperature determination by the spectroradiometry method, optical components of the system were selected to minimize the optical distortions (such as chromatic aberrations) and increase the bandwidth window of collected thermal radiation spectra to 570–830 nm. Due to the external control of the laser power, the energy of the laser pulse can be changed independently of its shape, as necessary for pulsed LH experiments. The flexibility and transportability of the system, as well as the possibility to couple it with various techniques at synchrotron facilities, have been successfully tested in a study of PdH behavior at high P-T conditions by means of powder X-ray diffraction and development of melting detection by XRTM on the beamline ID15B at the ESRF. The system can be assembled and aligned by users after basic training. All components of the system are commercially available, thus making it a ready solution for duplication.

ACKNOWLEDGMENTS

N.D. and L.D. thank the Federal Ministry of Education and Research, Germany (BMBF, Grant No. 5K16WC1) and the Deutsche Forschungsgemeinschaft (DFG Project Nos. DU 954-11/1, DU 393-9/2, and DU 393-13/1) for financial support.

A.S., A.B., and P.E. are very grateful for financial support by the Russian Science Foundation (Project No. 19-72-30009). A.B. expresses gratitude to the Russian Academic Excellence Project at the Immanuel Kant Baltic Federal University for the financial support for his travel.

REFERENCES

[1]W. A. Bassett, Rev. Sci. Instrum. **72**, 1270 (2001).
[2]W. A. Bassett, "Diamond anvil cells: Laser heating of samples at high pressure: 50 years," Laser Focus World, 2016, https://www.laserfocusworld.com/test-measurement/test-measurement/article/16547047/diamond-anvil-cells-laser-heating-of-samples-at-high-pressure-50-years.
[3]L. Liu, Geophys. Res. Lett. **1**, 277, https://doi.org/10.1029/gl001i006p00277 (1974).
[4]Y. Meng, R. Hrubiak, E. Rod, R. Boehler, and G. Shen, Rev. Sci. Instrum. **86**, 072201 (2015).
[5]B. Lavina, P. Dera, E. Kim, Y. Meng, R. T. Downs, P. F. Weck, S. R. Sutton, and Y. Zhao, Proc. Natl. Acad. Sci. U. S. A. **108**, 17281 (2011).
[6]L. Zhang, Y. Meng, W. Yang, L. Wang, W. L. Mao, Q.-S. Zeng, J. S. Jeong, A. J. Wagner, K. A. Mkhoyan, W. Liu, R. Xu, and H.-k. Mao, Science **344**, 877 (2014).
[7]W. L. Mao, Y. Meng, G. Shen, V. B. Prakapenka, A. J. Campbell, D. L. Heinz, J. Shu, R. Caracas, R. E. Cohen, Y. Fei, R. J. Hemley, and H.-k. Mao, Proc. Natl. Acad. Sci. U. S. A. **102**, 9751 (2005).
[8]R. Boehler, H. G. Musshoff, R. Ditz, G. Aquilanti, and A. Trapananti, Rev. Sci. Instrum. **80**, 045103 (2009).
[9]M. Mezouar, N. Rambert, G. Fiquet, D. Andrault, B. Sitaud, P. Loubeyre, S. Bauchau, W. Crichton, R. Boehler, E. Schultz, and G. Blattmann, High Press. Res. **25**, 71 (2007).
[10]G. Aquilanti, S. Pascarelli, O. Mathon, M. Muñoz, O. Narygina, and L. Dubrovinsky, J. Synchrotron Radiat. **16**, 376 (2009).
[11]C. Marini, I. Kantor, O. Mathon, and S. Pascarelli, High Press. Res. **33**, 108 (2013).
[12]J.-F. Lin *et al.*, Geophys. Res. Lett. **31**, L14611, https://doi.org/10.1029/2004GL020599 (2004).
[13]I. Kupenko, L. Dubrovinsky, N. Dubrovinskaia, C. McCammon, K. Glazyrin, E. Bykova, T. B. Ballaran, R. Sinmyo, A. I. Chumakov, V. Potapkin, A. Kantor, R. Rüffer, M. Hanfland, W. Crichton, and M. Merlini, Rev. Sci. Instrum. **83**, 124501 (2012).
[14]L. Dubrovinsky, K. Glazyrin, C. McCammon, O. Narygina, E. Greenberg, S. Übelhack, A. I. Chumakov, S. Pascarelli, V. Prakapenka, J. Bock, and N. Dubrovinskaia, J. Synchrotron Radiat. **16**, 737 (2009).
[15]T. Gu, X. Wu, S. Qin, and L. Dubrovinsky, Phys. Earth Planet. Inter. **184**, 154 (2011).
[16]O. Narygina, L. S. Dubrovinsky, H. Samuel, C. A. McCammon, I. Y. Kantor, K. Glazyrin, S. Pascarelli, G. Aquilanti, and V. B. Prakapenka, Phys. Earth Planet. Inter. **185**, 107 (2011).
[17]G. Aprilis, C. Strohm, I. Kupenko, S. Linhardt, A. Laskin, D. M. Vasiukov, V. Cerantola, E. G. Koemets, C. McCammon, A. Kurnosov, A. I. Chumakov, R. Rüffer, N. Dubrovinskaia, and L. Dubrovinsky, Rev. Sci. Instrum. **88**, 084501 (2017).
[18]See http://pishaper.com/geoheat.htm for Series of Lenses combining functions of Focusing the Laser Heating beam and spectroradiometric temperature measurements; Accessed 1 January 2019.
[19]B. D. Adams and A. Chen, Mater. Today **14**, 282 (2011).
[20]F. D. Manchester, A. San-Martin, and J. M. Pitre, J. Phase Equilib. **15**, 62 (1994).
[21]T. Skośkiewicz, M. Horobiowski, and E. Trojnar, J. Less Common Met. **101**, 311 (1984).
[22]T. Skoskiewicz, Phys. Status Solidi **11**, K123 (1972).
[23]H. M. Syed, T. J. Gould, C. J. Webb, and E. M. Gray, Prog. Solid State Chem. **44**, 20 (2016).
[24]K. Brownsberger, M. Ahart, M. Somayazulu, C. Park, S. A. Gramsch, and R. J. Hemley, J. Phys. Chem. C **121**, 27327 (2017).
[25]C.-S. Zha, K. Mibe, W. A. Bassett, O. Tschauner, H.-K. Mao, and R. J. Hemley, J. Appl. Phys. **103**, 054908 (2008).
[26]M. Santoro, J. F. Lin, V. Struzhkin, H. K. Mao, and R. J. Hemley, *Advances in High-Pressure Technology for Geophysical Applications* (Elsevier, 2005).
[27]L. Yang, Chin. Phys. B **25**, 076201 (2016).
[28]G. Shen and H. K. Mao, Rep. Prog. Phys. **80**, 016101 (2017).
[29]J. Ruiz-Fuertes, A. Karandikar, R. Boehler, and D. Errandonea, Phys. Earth Planet. Inter. **181**, 69 (2010).
[30]L. Yang, A. Karandikar, and R. Boehler, Rev. Sci. Instrum. **83**, 063905 (2012).
[31]S. Anzellini, A. Dewaele, M. Mezouar, P. Loubeyre, and G. Morard, Science **340**, 464 (2013).
[32]A. Salamat, R. A. Fischer, R. Briggs, M. I. McMahon, and S. Petitgirard, Coord. Chem. Rev. **277-278**, 15 (2014).
[33]D. Errandonea, B. Schwager, R. Ditz, C. Gessmann, R. Boehler, and M. Ross, Phys. Rev. B **63**, 132104 (2001).
[34]R. Jeanloz and A. Kavner, Philos. Trans. R. Soc. London, Ser. A: Math. Phys. Eng. Sci. **354**, 1279 (1996).
[35]R. Salem, S. Matityahu, A. Melchior, M. Nikolaevsky, O. Noked, and E. Sterer, Rev. Sci. Instrum. **86**, 093907 (2015).
[36]G. Aprilis, I. Kantor, I. Kupenko, V. Cerantola, A. Pakhomova, I. E. Collings, R. Torchio, T. Fedotenko, S. Chariton, M. Bykov, E. Bykova, E. Koemets, D. M. Vasiukov, C. McCammon, L. Dubrovinsky, and N. Dubrovinskaia, J. Appl. Phys. **125**, 095901 (2019).
[37]G. Morard, D. Andrault, D. Antonangeli, Y. Nakajima, A. L. Auzende, E. Boulard, S. Cervera, A. Clark, O. T. Lord, J. Siebert, V. Svitlyk, G. Garbarino, and M. Mezouar, Earth Planet. Sci. Lett. **473**, 94 (2017).
[38]N. Dubrovinskaia, L. Dubrovinsky, N. A. Solopova, A. Abakumov, S. Turner, M. Hanfland, E. Bykova, M. Bykov, C. Prescher, V. B. Prakapenka, S. Petitgirard, I. Chuvashova, B. Gasharova, Y.-L. Mathis, P. Ershov, I. Snigireva, and A. Snigirev, Sci. Adv. **2**, e1600341 (2016).
[39]A. Snigirev, P. Ershov, I. Snigireva, M. Hanfland, N. Dubrovinskaia, and L. Dubrovinsky, Microsc. Microanal. **24**, 238 (2018).
[40]A. Snigirev, V. Kohn, I. Snigireva, and B. Lengeler, Nature **384**, 49 (1996).

[41] G. B. M. Vaughan, J. P. Wright, A. Bytchkov, M. Rossat, H. Gleyzolle, I. Snigireva, and A. Snigirev, J. Synchrotron Radiat. **18**, 125 (2011).
[42] A. Snigirev, I. Snigireva, G. Vaughan, J. Wright, M. Rossat, A. Bytchkov, and C. Curfs, J. Phys. Conf. Ser. **186**, 012073 (2009).
[43] A. Narikovich, M. Polikarpov, A. Barannikov, N. Klimova, A. Lushnikov, I. Lyatun, G. Bourenkov, D. Zverev, I. Panormov, A. Sinitsyn, I. Snigireva, and A. Snigirev, J. Synchrotron Radiat. **26**, 1208 (2019).
[44] A. Bosak, I. Snigireva, K. S. Napolskii, and A. Snigirev, Adv. Mater. **22**, 3256 (2010).
[45] J.-M. Meijer, D. V. Byelov, L. Rossi, A. Snigirev, I. Snigireva, A. P. Philipse, and A. V. Petukhov, Soft Matter **9**, 10729 (2013).
[46] I. Snigireva, K. V. Falch, D. Casari, M. Di Michiel, C. Detlefs, R. Mathiesen, and A. Snigirev, Microsc. Microanal. **24**, 552 (2018).
[47] A. Kavner and R. Jeanloz, J. Appl. Phys. **83**, 7553 (1998).